Twenty-Seventh Symposium (International) on Combustion/The Combustion Institute, 1998/pp. 693–702

COMPUTATIONAL AND EXPERIMENTAL STUDY OF A FORCED, TIME-VARYING, AXISYMMETRIC, LAMINAR DIFFUSION FLAME

RAHIMA K. MOHAMMED, MICHAEL A. TANOFF,* MITCHELL D. SMOOKE, ANDREW M. SCHAFFER AND MARSHALL B. LONG

Department of Mechanical Engineering
Yale University
New Haven, CT 06520-8284, USA

Forced, time-varying flames are laminar systems that help bridge the gap between laminar and turbulent combustion. In this study, we investigate computationally and experimentally the structure of an acoustically forced, axisymmetric laminar methane-air diffusion flame in which a cylindrical fuel jet is surrounded by a coflowing oxidizer jet. The flame is forced by imposing a sinusoidal modulation on the steady fuel flow rate. Rayleigh scattering and spontaneous Raman scattering of the fuel are used to generate the temperature profile. Particle image velocimetry (PIV) is used to measure the fuel tube exit velocity over a cycle of the forcing modulation. CH flame emission measurements have been done to predict the excited-state CH (CH*) levels. Computationally, we solve the transient equations for the conservation of total mass, momentum, energy, and species mass with detailed transport and finite-rate C_2 chemistry submodels to predict the pressure, velocity, temperature, and species concentrations as a function of the two independent spatial coordinates and time. The governing equations are written in primitive variables. Implicit finite differences are used to discretize the governing equations and the boundary conditions on a nonstaggered, nonuniform grid. Modified damped Newton's method nested with a Bi-CGSTAB iteration is utilized to solve the resulting system of equations. Results of the study include a detailed description of the fluid dynamic-thermochemical structure of the flame at a 20-Hz frequency. A comparison of experimentally determined and calculated temperature profiles and CH* levels agree well. Calculated mole fractions of species indicative of soot production (C_2H_2, CO) are compared against those levels in the corresponding steady flame and are observed to increase in peak concentration values and spatial extent. Analysis of acetylene production rates reveals additional significant production in the downstream region of the flame at certain times during the flame's cyclic history.

Introduction

Most practical combustion systems, such as gas turbines and industrial furnaces, employ diffusion flames as the basic combustion element. These combustion systems are unsteady, high-speed, three-dimensional, turbulent reacting systems. A complete detailed understanding of the dynamical complexity of non-premixed turbulent reacting flows is beyond the capability of present computational models and experimental diagnostics. The last decade, however, has yielded significant progress in the study of multidimensional laminar steady diffusion flames both numerically and experimentally [1]. Time-varying laminar diffusion flames are another class of non-premixed combustion bridging the gap between steady laminar combustion and turbulent combustion. Time-varying flames offer a much wider range of interactions between chemistry and flow field than can be examined under steady-state conditions. The complex coupling between chemistry and fluid flow in time-varying laminar flames effectively samples different regimes of temperature, mixture fraction, residence time, strain, and scalar dissipation rates than are observed under steady conditions.

A specific type of unsteady flame, in which a periodic fluctuation in time is imposed on the fuel flow rate of a steady laminar flame, is known as a forced, time-varying flame. The study of these flames helps in understanding the interactions between fluid transport and heat and mass transfer in practical combustion systems. Fundamental studies of these interactions including detailed combustion chemistry are critical to the understanding of the pollutant formation processes and to the modeling of turbulent diffusion flames through the concept of laminar flamelets.

A number of investigations have considered laminar, time-varying diffusion flames. Some of these studies focused on naturally occurring flickering flames [2–6] and others on systems in which the fuel and air coflow were forced mechanically [7–16]. These investigations have been experimental

*Present address: The W.K. Kellogg Foundation, 2 Hamblin Ave. East, Battle Creek, MI 49016-3232.

[2,7–11], computational [5,6,12–14], or have combined both experimental and numerical techniques in their approach [3,4,15,16].

A number of these studies, primarily experimental, focused on the variation in soot production between steady and time-varying flames. For example, measurements have shown that the soot production in a forced, time-varying flame is four to five times greater than the soot production in a steady flame burning with the same mean fuel velocity [7–9]. In addition, quantitative two-photon laser-induced fluorescence imaging measurements of CO in forced, time-varying methane-air diffusion flames showed 50–65% larger volume-integrated CO levels [4]. Tunable diode laser absorption spectroscopy measurements of CO in a time-varying methane-air non-premixed flame indicated slightly higher concentrations over a broader region of space [11]. Computationally, Kaplan et al. [15] have solved the time-dependent, reactive flow equations coupled with submodels of soot formation and radiation transport for both steady and forced, time-varying CH_4-air diffusion flames. The computations utilized a methane consumption rate based on Bilger's mixture fraction formulation for chemical reaction in diffusion flames and computed four additional major chemical species based on their stoichiometric coefficients. These computations were compared against the experimental measurements of Shaddix and Smyth [8a,b].

In this study, we investigate computationally and experimentally the structure of a forced, time-varying, axisymmetric laminar methane-air diffusion flame in which a cylindrical fuel stream is surrounded by a coflowing oxidizer jet. Computationally, a primitive variable formulation with nonstaggered grids is used to solve the transient equations for the conservation of total mass, momentum, energy and individual chemical species mass to calculate the pressure, velocity, temperature, and species mass fractions as a function of space and time. This study is the first in which complex chemical kinetics are incorporated into a model to study forced, time-varying CH_4-air diffusion flames. Experimentally, Rayleigh scattering and Stokes-shifted Raman spectroscopy of the fuel are used to generate the temperature profile. Particle image velocimetry is used to measure the fuel tube exit velocity over a cycle of the forcing modulation. CH (CH*) flame emission measurements are used to predict the excited state CH levels. Our goals are to compare the different numerical and experimental spatial profiles of temperature and species concentrations at different times during a velocity cycle. In the next section, the experimental procedure is described. This is followed by the problem formulation and a description of the computational method. Finally, results of this investigation are discussed and concluded.

Experimental Procedure

Burner Configuration

Atmospheric pressure, overventilated, axisymmetric, coflowing, non-premixed laminar flames are generated with a burner in which the fuel flows from a 4.0-mm inner diameter vertical brass tube (wall thickness 0.38 mm) and the oxidizer flows from the annular region between this tube and a 50-mm-diameter concentric tube (see Fig. 1). The oxidizer is air, whereas the fuel is a mixture containing 65% methane and 35% nitrogen by volume. The nitrogen is added to help eliminate soot. The burner includes a small loudspeaker in the plenum of the fuel jet, which allows a periodic perturbation to be imposed on the exit parabolic velocity profile. Because the flame is lifted, there is no appreciable heat loss to the burner.

Laser Diagnostic Measurements

We obtain two-dimensional fields of temperature and fuel concentration using planar laser imaging, along with excited-state CH (CH*) emission. In addition, particle image velocimetry (PIV) is used to measure the fuel tube exit velocity over a cycle of the forcing modulation. The PIV experiment provides the inlet boundary conditions that are used in the computational studies. Rayleigh scattering and spontaneous Raman scattering of the fuel are used to determine the temperature field via the two-scalar approach of Stårner et al. [17]. The second harmonic of an Nd:YAG laser (532 nm) is focused into an 18-mm-tall vertical sheet over the center of the burner. The scattered light is collected perpendicular to the laser axis. The light passes through an appropriate interference filter and then is focused onto an intensified CCD camera using camera lenses. The laser and image intensifier are operated at a known phase delay with respect to the forcing of the flow; variation in the phase is made possible by electronic delay generators.

For Rayleigh scattering, a 532-nm interference filter (10-nm bandwidth) is used to isolate the scattering. Images acquired at two downstream locations are tiled together, resulting in an imaged region that extends from 4 to 40 mm off the surface of the burner. Laser energy is set to 100 mJ/pulse, and the scattering from 100 laser pulses (at a fixed phase relative to the forcing) is accumulated on the CCD. The forcing frequency of the flame is chosen to be 20 Hz, which is a multiple of the laser repetition rate (10 Hz) and which yielded an optimal response from the loudspeakers. Measurements are made at successive phase delays of 5 ms, allowing an entire cycle of the forced, time-varying flame to be represented as a series of 10 images.

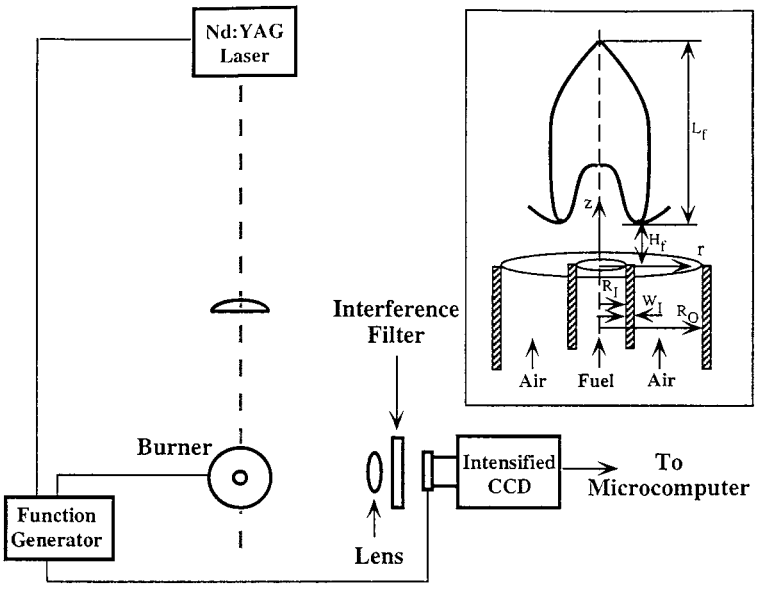

FIG. 1. Schematic of the experimental setup. Inset is the schematic of a forced, time-varying, unconfined, axisymmetric laminar diffusion flame.

A series of Stokes-shifted Raman images are acquired similarly to the Rayleigh images. A 630-nm (10-nm bandwidth) interference filter isolates the methane Raman scattering from the Rayleigh scattering. Laser energy is set to 210 mJ/pulse, and images are integrated for 600 laser shots. All images are corrected for optical throughput, background scattering, and nonuniformities in beam profile. Images are also corrected for flame luminosity and nonuniform detector response. By combining the Rayleigh and fuel Raman images that correspond to the same phase delay, the temperature is determined in an iterative manner [17].

For chemically excited CH (CH*) flame emission, the $A^2\Delta \rightarrow X^2\Pi$ transition occurs at 431.4 nm. CH* emission measurements are made by gating the image intensifier on for a period of 1 ms at varying phases with respect to the forcing. The object distance is increased to provide uniform magnification over the flame. The front camera lens is apertured down to $f/11$, and a narrow bandpass filter is used (center 431 nm, 10-nm bandwidth) for detection. Integrated, line-of-sight images of CH* emission are taken over 100 cycles of the forcing. These images are corrected for interferences from soot particulate emission by using another interference filter (center 700 nm, 10-nm bandwidth). The axisymmetric images were Abel inverted to obtain the relative CH* intensity from a cross section of the flame.

Problem Formulation

The time-varying axisymmetric laminar diffusion flame is modeled by solving the transient equations for the conservation of total mass, momentum, energy, and individual species mass. The system is closed with the ideal gas law and appropriate boundary conditions on each side of the computational domain. The initial conditions for the problem are the corresponding steady diffusion flame solution. The equations are written in two-dimensional, axisymmetric form in primitive variables (P, v_r, v_z, T, and Y_k, $k = 1, \ldots, n$, in which P is the total pressure, v_r is the radial velocity, v_z is the axial velocity, T is the temperature, Y_k is the species mass fraction, and n is the total number of species under investigation). This formulation allows for direct specification of velocity boundary conditions and is relatively straightforward to extend to 3-D. In the primitive variable formulation, however, it is difficult to choose the appropriate pressure boundary conditions, particularly because of the first-order nature of the pressure in the momentum equations and its absence from the continuity equation. Usually, a staggered grid arrangement is used to determine the discrete pressure field that is consistent with the discrete continuity equation. However, staggered mesh schemes have limitations in handling complex geometric configurations that require the use of nonorthogonal curvilinear coordinates. The nonstaggered grid has been applied in this formulation by using a one-sided difference approximation for the pressure gradient terms in the momentum conservation equations [18–20]. The one-sided difference avoids odd–even pressure decoupling that occurs from the use of a central difference approximation. The reduced accuracy of the one-sided differencing scheme is offset by nonuniform gridding.

For solving low-speed subsonic flows, we adopt an approach that splits the pressure field into the thermodynamic pressure (P_T) and the dynamic pressure (P_D) as $P_{\text{Total}} = P_T + P_D$ [21]. In our system, P_T is atmospheric pressure and P_D (which is computed) is approximately 0.003% of the thermodynamic pressure. Though very small in magnitude, it is the spatially varying dynamic pressure that drives the fluid flow. To avoid pressure waves reflecting back to the system, the thermodynamic pressure is used in the ideal gas law, and the $\partial P_D/\partial t$ term in the energy equation is neglected. We have also included an optically thin radiation model in our calculations and have assumed that for nonsooting methane-air mixtures, the only significant radiating species are H_2O, CO, and CO_2 [22].

Numerical Solution

The governing equations and boundary conditions are discretized by using an implicit finite-difference technique on a nine-point stencil. The implicit formulation allows for 3 orders of magnitude fewer time steps for describing the complete transient, as compared to explicit formulations [15]. Diffusion terms are approximated by centered differences and convective terms by a monotonicity-preserving upwind scheme. Thus, the partial differential equations are transformed into N_{eq} coupled nonlinear algebraic equations, where N_{eq} equals the number of unknowns multiplied by NODE, the number of mesh points in the computational domain. The resulting system of equations, written in residual form, is solved by a modified damped Newton's method [1]. A preconditioned (block Gauss–Seidel) bi-conjugate gradient stabilized (Bi-CGSTAB) method is used to solve the Newton equations [23]. The binary diffusion coefficients, viscosity, and thermal conductivity of the species and of the mixture, as well as the thermodynamic properties and the chemical production rates of the species, were evaluated using a set of vectorized and highly optimized chemistry and transport libraries [24].

Results and Discussion

In this section, we discuss the experimental and computational results for a forced, time-varying axisymmetric, unconfined, methane-air diffusion flame. Detailed transport coefficients and an 83-reaction, 26-species kinetic mechanism [25] were used in the calculations. As described in the inset of Fig. 1, the radii of the center fuel jet and the coflowing oxidizer jet are $R_I = 0.2$ cm and $R_O = 2.5$ cm, respectively, and the thickness of the fuel tube is $W_I = 0.038$ cm. The computational domain covers a region from $r = 0$ to $R_{\max} = 7.5$ cm in the radial direction and $z = 0$ to $z = 25$ cm in the axial direction. The dimensions of the domain are set to values much larger than the radius of the coflowing oxidizer jet, R_O, and the flame length, L_f, respectively, so that the asymptotic approach of the solution profile to its free-stream value can be predicted accurately. The fuel is nitrogen-diluted consisting of 65% CH_4 and 35% N_2. The time variation in the flame is produced by imposing a periodic velocity fluctuation on the fuel flow rate that has a parabolic profile with an average velocity of 35 cm/s.

Boundary conditions along the center line ($r = 0$) are such that v_r and radial gradients of all the other unknowns vanish. At the outer boundary ($r = R_{\max}$), the radial gradients of v_r and v_z vanish, the temperature is 298 K, and the mass fractions are specified as $Y_{O_2} = 0.232$, $Y_{N_2} = 0.768$, $Y_k = 0$, $k \neq O_2$, N_2. At the outflow boundary ($z = L$), P_T is atmospheric pressure, and the axial gradients of the remaining unknowns vanish. At the inflow boundary ($z = 0$), the radial velocity vanishes, and the temperature is 298 K. Across the fuel jet, $v_z = 70.0\ (1 - r^2/R_I^2)\ (1 + \alpha \sin \omega t)$ cm/s, where α is the velocity amplitude factor. The mass fractions at the inlet are $Y_{CH_4} = 0.5149$, $Y_{N_2} = 0.4851$, $Y_k = 0$, $k \neq CH_4$, N_2. The velocity across the oxidizer jet is 35 cm/s except for a thin boundary layer at the wall. Across the fuel tube thickness, W_I, and the region where $r > R_O$, v_z vanishes. For $R_I < r < R_{\max}$ at the inlet, the mass fractions are specified as $Y_{O_2} = 0.232$, $Y_{N_2} = 0.768$, $Y_k = 0$, $k \neq O_2$, N_2.

The computations have been performed on a nonuniform computational grid consisting of 91 × 82 cells in the radial (r) and axial (z) directions, respectively. We impose a 50% perturbation ($\alpha = 0.5$) on the steady parabolic fuel flow rate with a frequency of 20 Hz. In all the computed illustrations that follow, b corresponds to a peak inlet velocity of 61.6 cm/s at 0.01 s, c corresponds to a peak inlet velocity of 99.7 cm/s at 0.02 s, d corresponds to a peak inlet velocity of 98.6 cm/s at 0.03 s, e corresponds to a peak inlet velocity of 59.8 cm/s at 0.04 s, and f corresponds to a peak inlet velocity of 35.0 cm/s at 0.05 s.

In Figs. 2a–2f, we plot the computed isotherms of the steady and time-varying laminar CH_4-air diffusion flame. In Fig. 2a, the computed isotherms for the steady case are shown. The "wishbone" structure can be seen in the high-temperature region of the flame. The flame liftoff height, H_f, defined as the smallest z-coordinate at which $T \geq 1000$ K, is 0.66 cm. The maximum temperature at the center line is 1932 K at a height of 3.48 cm. The flame length L_f, defined as the difference between the location of the maximum temperature at the center line and the liftoff height, is 2.82 cm. A distinguishing feature of including the radiation model in the energy equation is that the peak temperature of 1947 K does not occur at the center line but in the "wings" at a radius

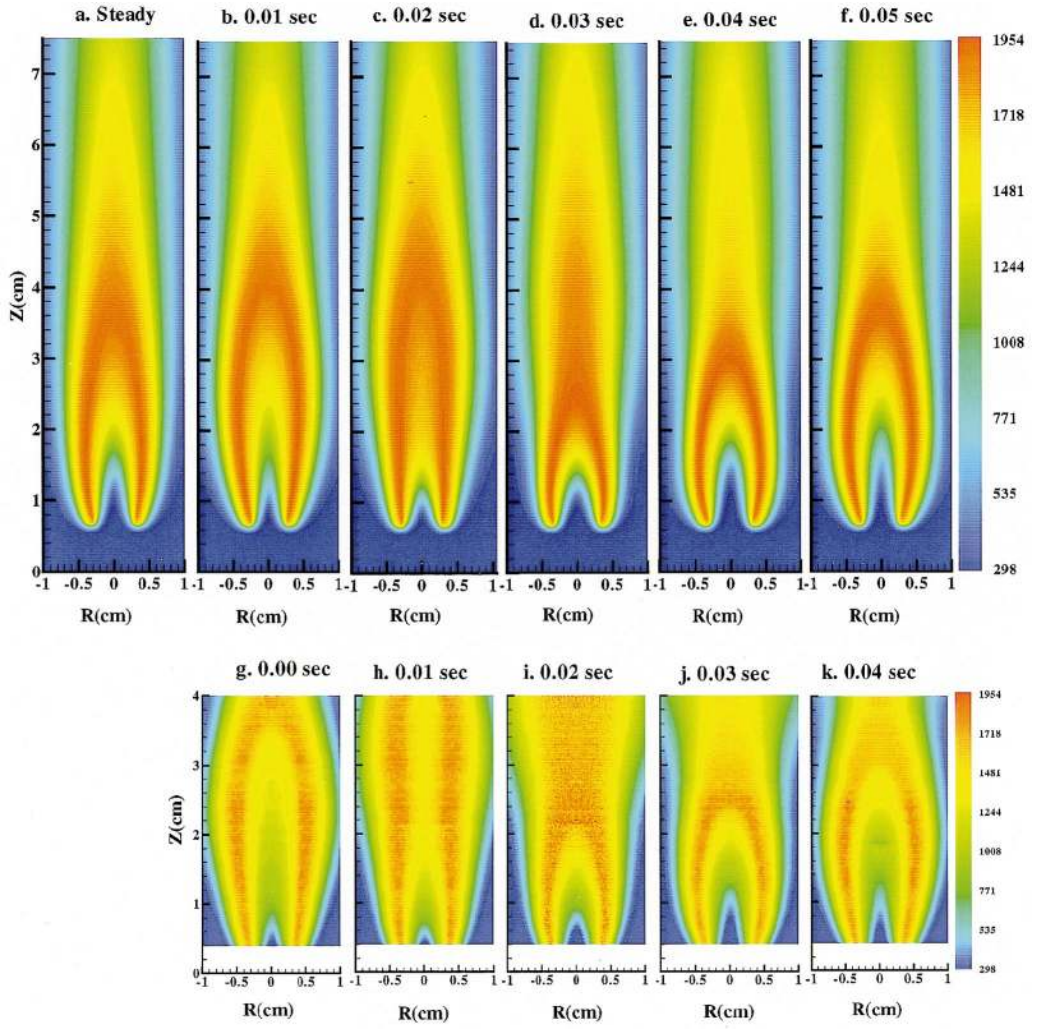

FIG. 2. Isotherms of the steady and time-varying laminar CH_4-air diffusion flame: (a) steady; (b–f) computed isotherms at 0.01, 0.02, 0.03, 0.04, and 0.05 s; (g–k) experimental isotherms at 0.00, 0.01, 0.02, 0.03, and 0.04 s.

of 0.37 cm. Peak CO_2, CO, and H_2O tend to occur on the center line, hence the radiation is the strongest there, and the temperature at the center line is lower. Without the radiation model, a maximum temperature of 2025 K occurs on the center line.

Figures 2b–2f are the computed isotherms of the time-varying flame at 0.01 s intervals (1/5 of the oscillation period). The simulations show that the oscillations imposed on the fuel flow rate induce similar oscillations on all the other variables. There is a phase difference between the axial velocity and the temperature. We also note that the isotherms in the part of the cycle where the velocity is rising (Figs. 2b and 2c) and in the part where the velocity is falling (Figs. 2d and 2e) are qualitatively different. In all the computed transient cases, the liftoff height is the same as in the steady-state case. However, the flame heights at the center line are 4.00, 4.00, 2.48, 2.97, and 3.60 cm. The overall length of the hot downstream plume of the flame is a better indicator of the forced oscillating nature of the flame. The structure of the flame deviates from the wishbone structure seen in the steady case. The transient behavior is very different from what we would expect to see in the steady-state case with similar mass flow rates of the fuel. In the steady-state case, the low-temperature core above the burner along the axis of symmetry increases and the overall length of the flame gets longer as the fuel mass flow rate is increased. In contrast, when the fuel flow rate is at its maximum (Fig. 2c), the low-temperature core is at its minimum. This behavior is due to the convective

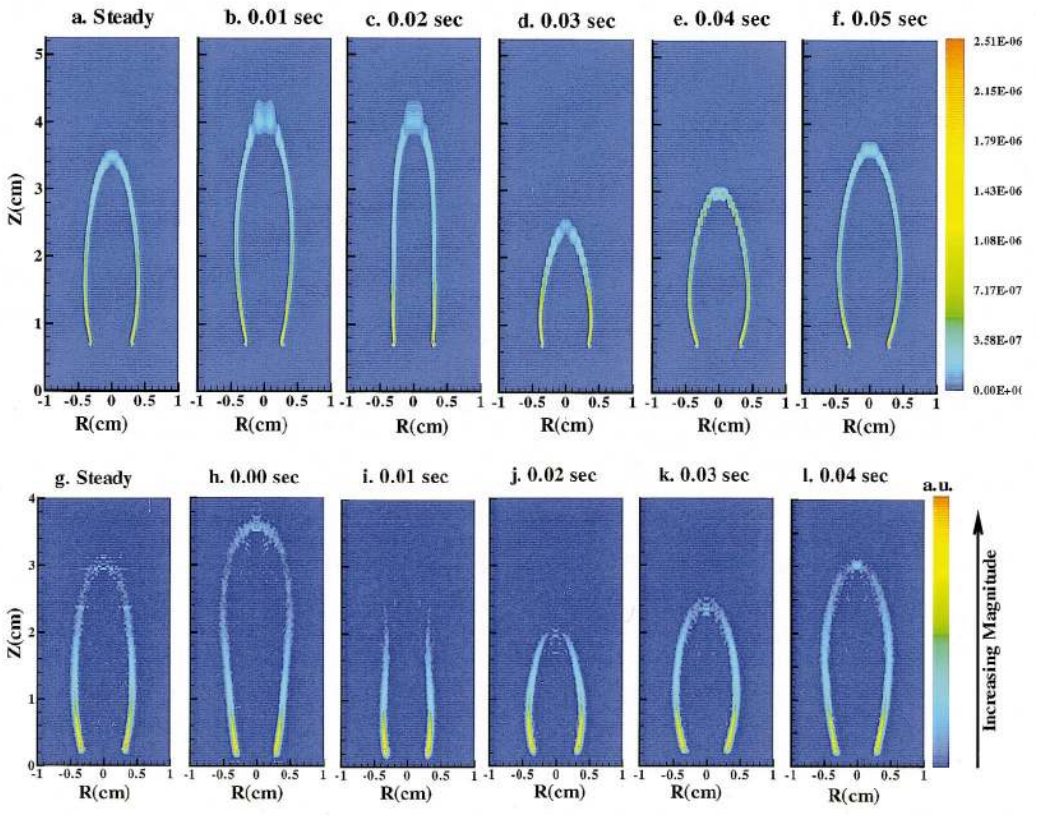

FIG. 3. CH mole fraction isopleths of the steady and time-varying laminar CH_4-air diffusion flame: (a) steady; (b–f) computed isopleths at 0.01, 0.02, 0.03, 0.04, and 0.05 s; (g–k) experimental isopleths at 0.00, 0.01, 0.02, 0.03, and 0.04 s.

timescales in the flame—during the time required for the effect of a fluid parcel at the inlet to convect to the flame height, the fuel velocity decreases to its minimum. The low-temperature core above the burner increases in length while the mean fuel velocity decreases (Figs. 2d and 2e). Hence, in the time-varying flame, the low-temperature core above the burner depends on the time history of the flame. Here, we can note, also, that the interior structure of the flame becomes elongated and noticeably less bowed. In the time-varying results, the peak temperature is 1954 K at a time of 0.03 s.

Figures 2g, 2h, 2i, 2j, and 2k represent the experimental temperature field measured by Rayleigh scattering and spontaneous Raman spectroscopy of the fuel at 0.00, 0.01, 0.02, 0.03, and 0.04 s, respectively. These figures are drawn to correspond to the computational results at 0.01, 0.02, 0.03, 0.04, and 0.05 s, respectively. The spatial features of the time-varying flame agree, quite well, qualitatively between the computations and the experiments. The profiles are shifted in time due to the convective timescale argument applied to the differences in liftoff height between the computations and the experiments. Experimentally, we measure a liftoff height that varies between 0.16 and 0.22 cm compared to a computational liftoff height of 0.66 cm. However, as our goal in future studies is an understanding of soot formation in forced, time-varying flames, we are particularly interested in the ability to predict accurately soot precursors such as C_2H_2. Although alternate kinetic schemes may produce better agreement in liftoff height, the present mechanism has been shown to predict excellent agreement between experimental and computational acetylene levels in counterflow and coflow flames [26,27].

Figure 3 represents the CH mole fraction isopleths for both the steady and time-varying case. The CH profile has the highest spatial activity of any of the 26 species considered in this study and is an excellent marker for the flame location and shape. Additionally, the CH radical is important in prompt NO_x formation in premixed and non-premixed methane-air systems. At steady state (Fig. 3a), the

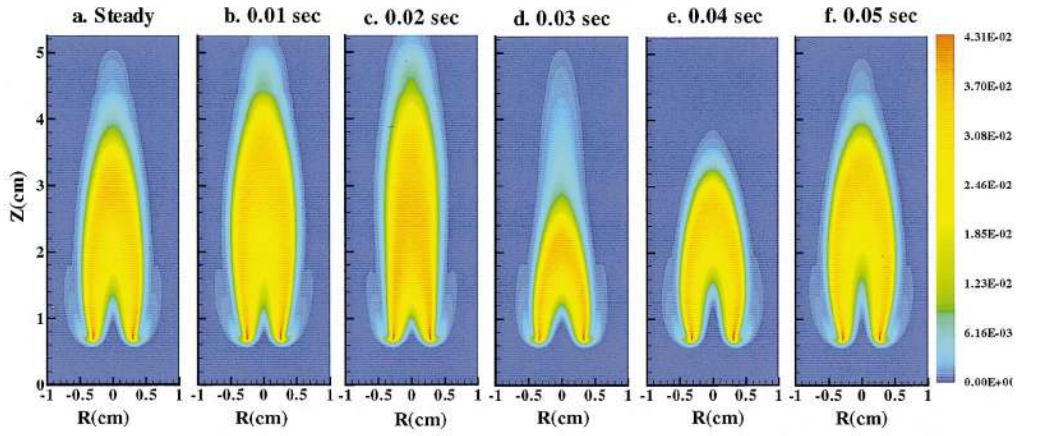

FIG. 4. CO mole fraction isopleths of the steady and time-varying laminar CH_4-air diffusion flame: (a) steady; (b–f) computed isopleths at 0.01, 0.02, 0.03, 0.04, and 0.05 s.

CH profile looks like an arch with the maximum near the open base. Figures 3b through 3f are the computed isopleths of the CH mole fraction of the time-varying flame. In Fig. 3c, where there is a maximum fuel flow rate, the inner structure looks more like an open cone at the top. In the part of the cycle where the velocity begins to decrease (Figs. 3d and 3e), the CH profiles look structurally similar, although wider, to the steady case. The peak mole fraction of CH is 1.25 times higher in the time-varying case in Fig. 3c than the steady case in Fig. 3a.

Figures 3g through 3k represent the experimental CH* flame emission measured at 0.01-s intervals. Experiments show that CH* concentrations are roughly 3 orders of magnitude lower than those of CH but are found to be spatially coincident. In both the experimental and computational illustrations, we can see a wider open base in Figs. 3d and 3j, respectively. Structurally, the computational results of the CH mole fraction and the experimentally obtained excited-state CH* emissions are in excellent agreement.

Figure 4 illustrates the isopleths of the CO mole fraction for both the steady and time-varying case. The CO concentration in time-varying laminar flames has been investigated previously [9,11]. It has been reported that increased amounts of soot in a time-varying flame result in larger concentrations of CO as well as depletion of OH radicals. In Fig. 4, again, we see that the isopleths in the part of the cycle where the velocity is rising (Figs. 4b and 4c) and in the part where the velocity is falling (Figs. 4d and 4e) are not the same. In Figs. 4b, 4e, and 4f, the CO profile resembles the steady profile but is wider. Hence, even though the peak mole fraction increases by at most 2% compared to the steady flame, the spatial region containing high CO levels is larger for the part of the cycle in which the velocity is increasing, as seen in previous experiments [9,11]. The CO profile in Fig. 4c with the maximum fuel flow rate becomes elongated and much less bowed.

In Fig. 5, we illustrate the computed acetylene mole fraction isopleths for a flame cycle. While the peak C_2H_2 mole fraction increases by 11.4% compared to the steady flame and varies by almost 36.0% during an oscillation, we observe that the region with the highest concentrations of this species can increase in spatial extent by more than a factor of 4 during a cycle. The highest mole fractions of acetylene occur when the inlet centerline axial velocity nears its peak (Fig. 5c). Figure 6 illustrates the corresponding molar chemical production rate isopleths for acetylene. The regions of highest production and destruction typically occur in a thin region along the flame front (similar profiles exist for CO and the other major species). However, at 0.04 s (Fig. 6e), we note additional significant acetylene production in the downstream region of the flame, which could lead to additional soot formation in the time-varying flame. Furthermore, from the moderately high flame temperatures, the absence of OH in the peak C_2H_2 region (low soot oxidation), the proportionality of inception and surface growth processes to C_2H_2 (see, for example, Refs. [28] and [29]), and the enhanced molar production rate of C_2H_2, it is clear that a forced, time-varying flame has the ability to produce significantly higher amounts of soot compared to unperturbed flames with the same average velocity.

Conclusions

In this paper, we have discussed a combined experimental and numerical solution of a forced, time-varying axisymmetric laminar diffusion flame. A two-scalar approach was used to measure the

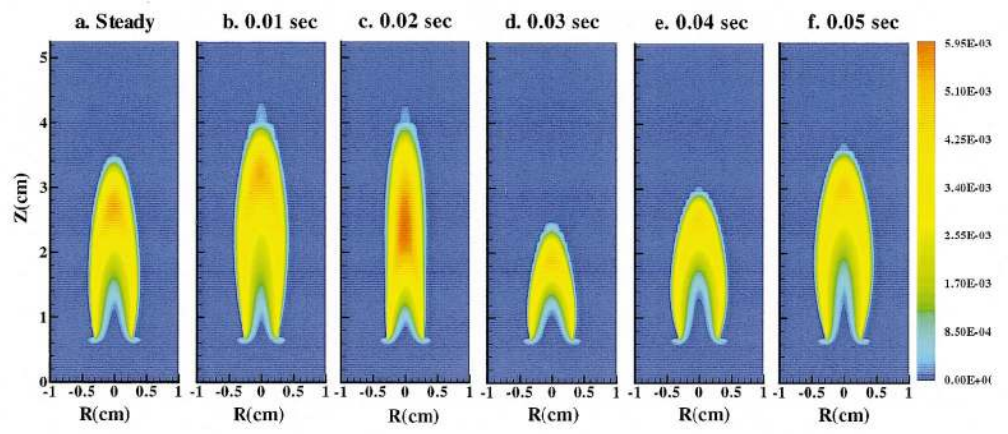

FIG. 5. C_2H_2 mole fraction isopleths of the steady and time-varying laminar CH_4-air diffusion flame: (a) steady; (b–f) computed isopleths at 0.01, 0.02, 0.03, 0.04, and 0.05 s.

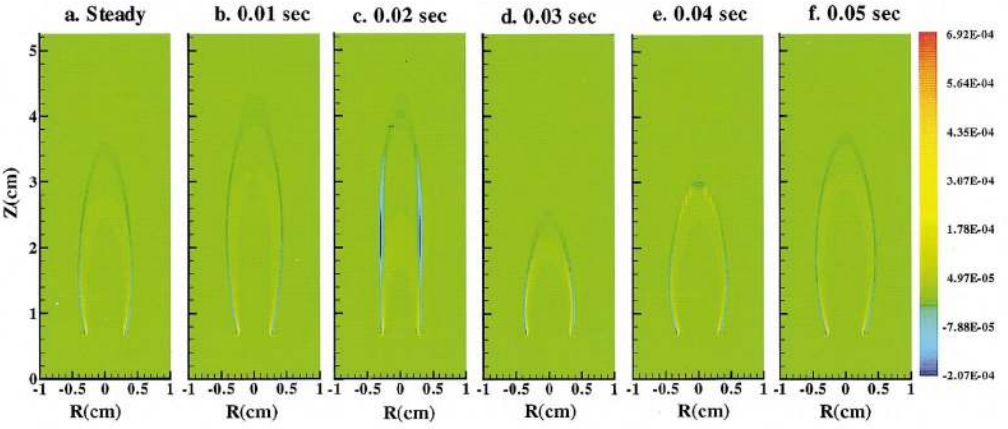

FIG. 6. C_2H_2 molar production (moles/cm^3 s) of the steady and time-varying laminar CH_4-air diffusion flame: (a) steady; (b–f) computed isopleths at 0.01, 0.02, 0.03, 0.04, and 0.05 s.

temperature. The two scalars were obtained by Rayleigh scattering and the measurement of fuel concentration via spontaneous Raman scattering. Particle image velocimetry was done to measure the fuel tube exit velocity over a cycle of the forcing modulation. CH* flame emission measurements have been done to show the overall flame shape and allow comparison with the computed CH profiles. Computationally, a fully transient detailed C_2 chemistry model of methane-air combustion was applied to a flame with a forcing frequency of 20 Hz. The overall structure of the temperature and CH profiles predicted by the computations were in very good qualitative agreement with the experimental measurements. Previous researchers have shown that soot production in a forced time-varying flame is four to five times greater than the soot production in a steady flame burning with the same mean fuel velocity. To investigate this issue, we examined species indicative of soot production, CO and C_2H_2. We find that the peak C_2H_2 mole fraction increases by 11.4% compared to the steady flame and varies as much as 36% during an oscillation. More importantly, the region with the highest C_2H_2 species concentration can increase in spatial extent by a factor of 4 during a cycle, and additional significant acetylene production occurs in a downstream region of the flame during certain times in the cycle. In order to gain additional insight into soot formation in these flames, the current kinetic model should be modified to include ring formation chemistry similar to that in Ref. [29]. In addition, it is clear from the current study that further investigation is needed into the effects of the magnitude and the frequency of the velocity

perturbations on the flame structure. Ultimately, a soot formation model will be incorporated into the current gas-phase system.

Acknowledgment

The authors gratefully acknowledge support for this research from the Department of Energy under Grant Number DE-FG02-88ER-13966.

REFERENCES

1. Xu, Y., Smooke, M. D., Lin, P., and Long, M. B., *Combust. Sci. Technol.* 90:289–313 (1993).
2. Chen, L. D., Seaba, J. P., Roquemore, W. M., and Goss, L. P., in *Twenty-Second Symposium (International) on Combustion,* The Combustion Institute, Pittsburgh, 1988, pp. 677–684.
3. Davis, R. W., Moore, E. F., Roquemore, W. M., Chen, L. D., Vilimpoc, V., and Goss, L. P., *Combust. Flame* 83:263–270 (1991).
4. Katta, V. R., Goss, L. P., and Roquemore, W. M., *Combust. Flame* 96:60–74 (1994).
5. Ellzey, J. L. and Oran, E. S., in *Twenty-Third Symposium (International) on Combustion,* The Combustion Institute, Pittsburgh, 1991, pp. 1635–1641.
6. Kaplan, C. R., Baek, S. W., Oran, E. S., and Ellzey, J. L., *Combust. Flame* 96:1–21 (1994).
7. Smyth, K. C., Harrington, J. E., Johnson, E. L., and Pitts, W. M., *Combust. Flame* 95:229–239 (1993).
8. Shaddix, C. R. and Smyth, K. C., *Combust. Flame* 99:723–732 (1994), 100:518 (1995), and 107:418–452 (1996).
9. Everest, D. A., Shaddix, C. R., and Smyth, K. C., in *Twenty-Sixth Symposium (International) on Combustion,* The Combustion Institute, Pittsburgh, 1996, pp. 1161–1169.
10. Smyth, K. C., Shaddix, C. R., and Everest, D. A., *Combust. Flame* 111:185–207 (1997).
11. Skaggs, R. R. and Miller, J. H., in *Twenty-Sixth Symposium (International) on Combustion,* The Combustion Institute, Pittsburgh, 1996, pp. 1181–1188.
12. Mahalingam, S., Cantwell, B. J., and Ferziger, J. H., *Phys. Fluids A* 2:301–312 (1990).
13. Egolfopoulos, F. N. and Campbell, C. S., *J. Fluid Mech.* 318:1–29 (1996).
14. Pember, R. B., Howell, L. H., Bell, J. B., Collela, P., Crutchfield, W. Y., Fiveland, W. A., and Jessee, J. P., *Western States Section of the Combustion Institute, 1997 Fall Meeting,* 1997.
15. Kaplan, C. R., Shaddix, C. R., and Smyth, K. C., *Combust. Flame* 106:392–405 (1996).
16. Najm, H. N., Schefer, R. W., Milne, R. B., Mueller, C. J., Devine, K. D., and Kempka, S. N., *Sandia National Laboratories report,* SAND98-8232, 1998.
17. Stårner, S., Bilger, R. W., Dibble, R. W., and Barlow, R. S., *Combust. Sci. Technol.* 86:223–236 (1992).
18. Abdallah, S., *J. Comput. Phys.* 70:182–192 (1987) and 70:193–202 (1987).
19. Armfield, S. W., *Comput. Fluids* 20:1–17 (1991).
20. Babu, V. and Korpela, S. A., *Comput. Fluids* 23:675–691 (1994).
21. Majda, A. and Sethian, J. A., *Combust. Sci. Technol.* 42:187–205 (1985).
22. Hall, R. J., *J. Quant. Spectros. Radiat. Transfer* 49:517–523 (1993) and 51:635–644 (1994).
23. van der Vorst, H. A., *SIAM J. Sci. Stat. Comput.* 13:631–644 (1992).
24. Giovangigli, V. and Darabiha, N., in *Mathematical Modeling in Combustion and Related Topics* (C.-M. Brauner and C. Schmidt-Lainé, eds.), 491–503 Martinus Nijhoff Publishers, Dordrecht, 1988, pp. 491–503.
25. Smooke, M. D., Xu, Y., Zurn, R. M., Lin, P., Frank, J. H., and Long, M. B., in *Twenty-Fourth Symposium (International) on Combustion,* The Combustion Institute, Pittsburgh, 1992, pp. 813–821.
26. Smooke, M. D., McEnally, C. S., Pfefferle, L. D., Hall, R. J., and Colket, M. B., "Computational and Experimental Study of Soot Formation in a Coflow, Laminar Diffusion Flame," *Combust. Flame,* in press.
27. Puri, I., Seshadri, K., Smooke, M. D., and Keyes, D. E., *Combust. Sci. Technol.* 56:1–22 (1987).
28. Fairweather, M., Jones, W. P., and Lindstedt, R. P., *Combust. Flame* 89:45–63 (1992).
29. Hall, R. J., Smooke, M. D., and Colket, M. B., "Predictions of Soot Dynamics in Opposed Jet Diffusion Flames," in *Physical and Chemical Aspects of Combustion: A Tribute to Irvin Glassman* (R. F. Sawyer and F. L. Dryer, eds.), Combustion Science and Technology Book Series, Gordon and Breach, 1997.

COMMENTS

Houston Miller, George Washington University, USA.

1. In some of your image comparisons, the computed temperature field appeared broader than the experimentally determined profiles. If this observation is true, have you varied the forcing amplitude and followed the resulting change in flame width?
2. Your model does not yet include soot growth and oxidation. In our paper [1], we conjectured that soot oxidation was at least partially responsible for enhanced CO levels. Could you comment on how CO production from PAH and soot oxidation might impact your results?

REFERENCE

1. Skaggs, R. R. and Miller, J. H., in *Twenty-Sixth Symposium (International) on Combustion*, The Combustion Institute, Pittsburgh, 1996, pp. 1181–1188.

Author's Reply.

1. We have performed computations in which the velocity was perturbed form a low of 25% to a high of 75% of its average value. Higher velocity perturbations produce temperature profiles that can vary dramatically in shape during a complete velocity cycle. The overall maximum width in the temperature during a cycle is similar regardless of the level of the perturbation.
2. The issue of enhanced CO production is extremely interesting and one that we are actively studying. While we agree that soot oxidation can enhance CO levels, the best way to answer your question is to interrogate a transient solution, including the soot field, assuming predicated soot levels are comparable to experimental values. However, we believe that the effect will be somewhat mitigated since the peak soot levels are lower in our flame compared to those observed in yours.

•

Makihito Nishioka, University of Tsukuba, Japan. I think that the temperature of the burner rim affects the lift-off height significantly. Because there is a large difference of the lift-off height between the calculation and the experiment, how did you give the temperature boundary condition at the rim?

Author's Reply. You are correct in stating that the temperature of the burner rim affects the lift-off height. For example, lower lift-off heights imply higher rim temperatures and vice versa. The temperature of the rim in our computation was specified at 298 K. We believe that the difference in the lift-off height between the experiments and the calculations is due to a flow modification in the burner coflow.